

Bilevel Learning via Inexact Stochastic Gradient Descent *

Mohammad Sadegh Salehi[†], Subhadip Mukherjee[‡], Lindon Roberts[§], and
Matthias J. Ehrhardt [¶]

Abstract. Bilevel optimization is a central tool in machine learning for high-dimensional hyperparameter tuning. Its applications are vast; for instance in imaging it can be used for learning data-adaptive regularizers and optimizing forward operators in variational regularization. These problems are large in many ways: a lot of data is usually available to train a large number of parameters, calling for stochastic gradient-based algorithms. However, due to the nature of the problem, exact gradients with respect to the parameters (so-called hypergradients) are not available. In fact, the precision of the hypergradient is usually linearly related to the cost, thus requiring algorithms which can solve the problem without requiring unnecessary precision. However, the design of such algorithms is still not fully understood, especially in terms of how accuracy requirements and step size schedules influence both theoretical guarantees and practical performance. Existing approaches often introduce stochasticity at both the upper level (e.g., in sampling or mini-batch gradient estimates for the outer objective) and the lower level (e.g., in approximating the solution of the inner optimization problem), to improve generalization. At the same time, they typically enforce a fixed number of lower-level iterations, which does not align with the assumptions underlying asymptotic convergence analysis. In this work, we advance the theoretical foundations of inexact stochastic bilevel optimization. We prove convergence and establish rates under both decaying accuracy and step size schedules, showing that, with optimal configurations, convergence occurs at an $O(k^{-1/4})$ rate in expectation. Experiments on image denoising and inpainting with convex ridge regularizers and input-convex networks confirm our analysis: decreasing step sizes improves stability, accuracy scheduling is more critical than step size strategy, and adaptive preconditioning (e.g., Adam) further boosts performance. These results help bridge the gap between theory and practice in bilevel optimization, providing convergence guarantees and practical guidance for large-scale imaging problems.

Key words. Bilevel Learning, Bilevel Optimization, Stochastic Optimization, Learning Regularizers, Machine Learning, Variational Regularization, Imaging, Inverse Problems.

MSC codes. 65K10, 90C25, 90C26, 90C06, 90C31, 94A08

*Submitted to the editors DATE.

Funding: MSS acknowledges support from the EPSRC Centre for Doctoral Training in Statistical Applied Mathematics at Bath (SAMBa), under the project EP/S022945/1. MJE acknowledges support from the EPSRC (EP/T026693/1, EP/V026259/1, EP/Y037286/1) and the European Union Horizon 2020 research and innovation programme under the Marie Skłodowska-Curie grant agreement REMODEL.). LR is supported by the Australian Research Council Discovery Early Career Award DE240100006. SM acknowledges support from the ANRF under the Prime Minister Early Career Research Grant program (ANRF/ECRG/2024/001178/ENS).

[†]Independent Researcher, Bath, UK (sadeghsalehi1997@gmail.com).

[‡]Department of Electronics & Electrical Communication Engineering, Indian Institute of Technology (IIT), Kharagpur, India (smukherjee@ece.iitkgp.ac.in).

[§]School of Mathematics and Statistics, University of Melbourne, Parkville VIC 3010, Australia (lindon.roberts@unimelb.edu.au).

[¶]Department of Mathematical Sciences, University of Bath, Bath, BA2 7AY, UK (m.ehrhardt@bath.ac.uk).

1. Introduction.

1.1. Problem motivation. Bilevel optimization has become a versatile tool in machine learning and inverse problems, particularly in imaging applications where the quality of reconstruction depends critically on the choice of regularization parameters that encode the image prior. In variational regularization, the lower-level problem typically takes the form

$$\min_{x \in \mathbb{R}^n} \{h(x, \theta) := D(Ax, y) + R_\theta(x)\},$$

where D denotes a data fidelity term, A is a forward operator, y is the noisy measurement, and R_θ is a parametric regularizer. The upper-level problem then optimizes the parameter θ to minimize a supervised loss, yielding a nested optimization structure that can adapt regularizers to specific datasets. This framework has proven effective for learning data-adaptive priors in imaging inverse problems [34, 21, 22, 26]. It can also be used to optimize physical acquisition models, such as sampling strategies in MRI reconstruction [48, 51], and to design forward models in seismic imaging [13], by parameterizing the forward operator A with a learnable parameter θ .

In this work, we consider the stochastic bilevel optimization problem

$$(1.1a) \quad \min_{\theta} \mathbb{E}_{v \sim \mathcal{D}} \left[f_v(\theta) := \frac{1}{m} \sum_{i=1}^m v_i f_i(\theta) = \frac{1}{m} \sum_{i=1}^m v_i g_i(\hat{x}_i(\theta)) \right],$$

$$(1.1b) \quad \text{s.t. } \hat{x}_i(\theta) := \arg \min_{x \in \mathbb{R}^n} h_i(x, \theta), \quad i = 1, 2, \dots, m,$$

where $v \in \mathbb{R}^m$ is a sampling vector with independent entries, e.g., $v_i \sim \text{Binomial}(m, 1/m)$, and $\mathbb{E}[v_i] = 1$ for all $i \in \{1, 2, \dots, m\}$. The upper-level functions g_i measure the quality of the lower-level solutions, e.g., $g_i(x) = \|x - x_i^*\|^2$ with x_i^* denoting the desired solution. Note that in case we have access to the exact lower-level solution $\hat{x}_i(\theta)$ for all $i \in \{1, 2, \dots, m\}$, f_v and ∇f_v are the unbiased estimators of f and ∇f , respectively, i.e., $\mathbb{E}_{v \sim \mathcal{D}}[f_v(\theta)] = f(\theta)$ and $\mathbb{E}_{v \sim \mathcal{D}}[\nabla f_v(\theta)] = \nabla f(\theta)$.

Despite its theoretical appeal, large-scale bilevel optimization presents significant computational challenges. Computing the exact solution of the lower-level problems $\hat{x}_i(\theta)$ is typically intractable, and as a result, practical algorithms must rely on inexact solutions, which in turn yield approximate hypergradients that can significantly influence convergence behavior [37]. Moreover, the approximation of the hypergradient leads to biased estimator, which necessitates a careful analysis of convergence behavior [46].

1.2. Related work. Derivative-free methods have been proposed to mitigate the computational complexities arising in approximations [15, 49], sometimes incorporating adaptive or stochastic strategies. However, their scalability is limited when the number of parameters is large. By contrast, gradient-based bilevel methods offer better scalability [32, 18, 24, 45], but existing approaches predominantly focus on deterministic formulations [36, 51, 50, 45] and therefore do not fully exploit the speed-up and generalization benefits of stochastic optimization [46].

A complementary line of work has analyzed approximate hypergradients under different regularity assumptions, both a priori and a posteriori [16, 33, 24, 25, 5, 3]. However, algorithms

that rely on these approximations usually fix the number of lower-level iterations [39, 38, 27, 29] and assume asymptotic convergence with a constant upper-level step size. This mismatch creates a gap between theoretical guarantees and practical implementations. Although recent work has investigated realistic assumptions for stochastic gradients [23, 28, 11], extending these insights to bilevel optimization remains an open direction.

Other relevant works exploit hypergradient subroutines, such as approximating the inverse Hessian, to improve computational efficiency [14, 39]. Jacobian-free approaches [19, 6, 47, 52], also known as truncated backpropagation, provide a memory-efficient alternative to unrolling [35, 18]. Instead of solving a linear system to approximate the inverse Hessian, these methods approximate it via backpropagation of a single iteration.

A series of works have focused on efficient learning data-adaptive regularizers for inverse problems, developing cost-reduced, accuracy-dependent, and adaptive bilevel methods [45, 4]. These methods have also been successfully applied in related contexts such as deep image priors [44] and experimental design [17], demonstrating both effectiveness and computational speed-ups while maintaining theoretical soundness. In parallel, single-step approaches [12, 51] have introduced cost-reduced bilevel algorithms in a non-adaptive setting. However, both adaptive and single-step approaches remain deterministic and are therefore limited to smaller datasets. More recently, [46] introduced inexact stochastic hypergradients and established convergence guarantees by drawing connections to biased stochastic gradient descent. While this marked an important first step toward scalable stochastic bilevel methods in imaging, several key questions were left open. In particular, the effects of decaying step size and accuracy schedules on convergence were not addressed, nor were convergence rates established. Furthermore, the practical interaction between these schedules remained unexplored.

By considering the solver of the lower-level problem as fixed-point iterations of a contraction map, the Deep Equilibrium (DEQ) framework [10, 7, 9] provides a more general perspective, where implicit-function-theorem (IFT) based bilevel approaches arise as a special case. In these methods, the solution is characterized as a fixed point of a nonlinear operator, and practical work has largely focused on performance while relaxing formal convergence guarantees. The upper-level solver is typically chosen to be Adam [30] with a tuned step size, leaving many theoretical questions regarding accuracy and step size schedules unaddressed. Analyzing DEQ under inexact fixed-point computations therefore naturally subsumes the IFT-based bilevel case, while also highlighting that advances in one viewpoint can transfer to the other.

1.3. Contributions. This work extends the theoretical foundation of inexact stochastic bilevel optimization by establishing explicit convergence rates under polynomial and logarithmic accuracy and step size decay schedules. Our analysis reveals that optimal theoretical performance is achieved with accuracy decay $\epsilon_k = \mathcal{O}(k^{-1/4})$ and step size decay $\alpha_k = \mathcal{O}(k^{-1/2-\delta})$ with $0 < \delta < 0.5$ (optimally when $\delta \approx 0$), yielding convergence rates of $\mathcal{O}(k^{-1/4})$. For comparison, this matches the convergence rate of stochastic gradient descent for smooth nonconvex functions, where the expected squared gradient norm decays as $\mathcal{O}(k^{-1/2})$, corresponding to $\mathcal{O}(k^{-1/4})$ in terms of the expected gradient norm [20]. Building on this result, we numerically investigate different accuracy and step size schedules, including fixed step sizes that guarantee only neighborhood convergence [1, 46], to assess their practical performance under finite

computational budgets.

Through comprehensive numerical experiments on image denoising and inpainting with multiple regularizer architectures, namely Convex Ridge Regularizers (CRR) [21] and Input-Convex Neural Networks (ICNN) [34] we uncover several key insights that bridge the gap between theory and practice. First, accuracy scheduling is more critical than step size strategy for achieving a desirable performance. Second, while decreasing step sizes are required for asymptotic convergence guarantees, fixed step sizes often yield superior results in practice under limited budgets, suggesting opportunities for an improved non-asymptotic analysis. Third, adaptive optimization methods such as Adam [30] substantially outperform standard SGD [42], particularly for more complex regularizer architectures. Adam achieves this by combining a moving average of the stochastic gradients, which induces a momentum effect, with a coordinate-wise rescaling akin to preconditioning. This highlights the importance of incorporating both mechanisms in bilevel optimization.

Our empirical findings reveal a nuanced relationship between theoretical optimality and practical performance. While the theoretically optimal parameter configuration provides stability and convergence guarantees, more aggressive accuracy decay or fixed step sizes often deliver superior results under finite computational budgets. These results demonstrate that asymptotically optimal schedules do not necessarily translate into the best finite-time performance, underscoring the practical relevance of our analysis for guiding parameter choices in bilevel learning algorithms.

The remainder of this paper is organized as follows. Section 2 introduces the theoretical and algorithmic framework, including the assumptions and lemmas required for our analysis. Section 3 presents the convergence results and establishes the associated rates. Section 4 reports comprehensive numerical experiments across multiple imaging tasks and regularizer architectures. Finally, Section 5 concludes with practical guidelines and directions for future research.

2. Proposed method. Considering the upper-level problem (1.1a), the gradient of the upper-level objective, called the *hypergradient*, is given by

$$(2.1) \quad \mathbb{E}_{v \sim \mathcal{D}} \left[\nabla f_v(\theta) := \frac{1}{m} \sum_{i=1}^m v_i \nabla f_i(\theta) = \frac{1}{m} \sum_{i=1}^m v_i \partial \hat{x}_i(\theta)^T \nabla g_i(\hat{x}_i(\theta)) \right].$$

To ensure the hypergradient is well-defined (i.e., $\hat{x}_i(\theta)$ is continuously differentiable), it suffices to assume that each lower-level function $h_i(x, \theta)$ is strongly convex in x and continuously differentiable, with its first and second derivatives with respect to x continuous in θ . In addition, each upper-level loss g_i is assumed to be continuously differentiable.

Each iteration $k \in \mathbb{N}$ of SGD takes the following form

$$(2.2) \quad \theta^{k+1} = \theta^k - \alpha_k \nabla f_{v^k}(\theta^k),$$

where $v^k \sim \mathcal{D}$ are independent and identically distributed (i.i.d.) and $\alpha_k > 0$ is the step size.

Since, in general, the lower-level solution $\hat{x}_i(\theta^k)$ at each upper-level iteration $k \in \mathbb{N}$ can only be approximated, one typically has access only to the approximate lower-level solution

$\tilde{x}_i(\theta^k)$, where

$$\|\hat{x}_i(\theta^k) - \tilde{x}_i(\theta^k)\| \leq \epsilon.$$

Hence, corresponding to each element v_i^k of the sampling vector v^k for all $i \in \{1, 2, \dots, m\}$, the stochastic hypergradient $v_i^k \partial \hat{x}_i(\theta^k)^T \nabla g_i(\hat{x}_i(\theta^k))$ can be approximated using methods described in [16, 33] with an error of $\mathcal{O}(\epsilon)$. This results in an inexact stochastic hypergradient in the upper-level problem, which we denote by

$$(2.3) \quad z_k = z_{v^k}(\theta^k) = \nabla f_{v^k}(\theta^k) + e_{v^k}(\theta^k) \quad v^k \sim \mathcal{D}.$$

Note that ensuring the boundedness of this error can be done utilizing the error bounds provided in [16, 24]. Putting these ingredients together results in the proposed algorithm Inexact Stochastic Gradient Descent (ISGD), see [Algorithm 2.1](#).

Algorithm 2.1 Inexact Stochastic Gradient Descent (ISGD) with varying step size and accuracy

- 1: Input: Initial parameters $\theta^0 \in \mathbb{R}^d$, sampling \mathcal{D} , positive step size sequence $\{\alpha_k\}_{k=0}^\infty$, non-negative accuracy sequence $\{\epsilon_k\}_{k=0}^\infty$.
- 2: **for** $k = 0, 1, \dots$ **do**
- 3: Sample a mini-batch $v^k \sim \mathcal{D}$.
- 4: Compute the approximate stochastic gradient $z_{v^k}(\theta^k)$ with error $\mathcal{O}(\epsilon_k)$.
- 5: Update the iterate:

$$(2.4) \quad \theta^{k+1} = \theta^k - \alpha_k z_{v^k}(\theta^k)$$

Before presenting the full analysis, we summarize the main convergence result of ISGD.

Theorem 2.1 (Convergence Preview). *Under Assumptions 3.1–3.3 and a sufficiently small initial step size $\alpha_0 > 0$, the iterates $\{\theta^k\}$ generated by [Algorithm 2.1](#) satisfy*

$$(2.5) \quad \min_{0 \leq k \leq K-1} \mathbb{E}[\|\nabla f(\theta^k)\|^2] \leq \frac{C_1}{K\alpha_K} + C_2 L_K, \quad L_K := \frac{1}{K\alpha_K} \sum_{k=0}^{K-1} \alpha_k \epsilon_k^2,$$

for some constants $C_1, C_2 > 0$. If $L_K \rightarrow 0$, then $\mathbb{E}[\|\nabla f(\theta^k)\|] \rightarrow 0$ as $K \rightarrow \infty$.

In particular, for step sizes $\alpha_k = \mathcal{O}(k^{-q})$ with $\frac{1}{2} < q < 1$ and accuracies $\epsilon_k = \mathcal{O}(k^{-p})$ with $p > 0$, we have

$$(2.6) \quad \min_{0 \leq k \leq K-1} \mathbb{E}[\|\nabla f(\theta^k)\|] = \mathcal{O}\left(K^{-\frac{1}{2} \min\{2p, 1-q\}}\right).$$

The detailed convergence theorem and the corresponding convergence rate analysis are presented in [Theorem 3.10](#) and [Corollary 3.13](#), respectively.

Insight. ISGD converges in expectation to a stationary point of the bilevel objective. The rate in (2.6) matches that of standard SGD [41] when the hypergradient error decays sufficiently fast (i.e., p is sufficiently large), but can be slower if the accuracy is not improved at a fast enough rate.

3. Convergence analysis. To prove the convergence of [Algorithm 2.1](#), we make the following regularity assumptions.

Notation. For any $v \sim \mathcal{D}$ and for all $\theta \in \mathbb{R}^d$, the error of the hypergradient is denoted by $\|e_v(\theta)\|$ and the expected squared error by $E^2(\theta) := \mathbb{E}_{v \sim \mathcal{D}}[\|e_v(\theta)\|^2]$. Moreover, at each iteration $k \in \mathbb{N}$ of [Algorithm 2.1](#), we denote the hypergradient approximation given a sample v^k and parameters θ^k by $z_k := z_{v^k}(\theta^k)$.

Assumption 3.1. Each f_i is $L_{\nabla f_i}$ -smooth, which means f and each f_i are continuously differentiable with $L_{\nabla f}$ and $L_{\nabla f_i}$ Lipschitz gradients, respectively. Moreover, each f_i is bounded below by f_i^{\inf} .

Since, in practice, in each iteration $k \in \mathbb{N}$ of [Algorithm 2.1](#), the error $\|e_{v^k}(\theta^k)\|$ is controlled by a deterministic a posteriori upper bound, we consider the following assumption.

Assumption 3.2. At each iteration $k \in \mathbb{N}$ of [Algorithm 2.1](#), for the error of the hypergradient we have $\mathbb{E}_{v^k \sim \mathcal{D}}[\|e_{v^k}(\theta^k)\|^2] \leq \epsilon_k^2$, where $\{\epsilon_k\}_{k=0}^\infty$ is a deterministic non-negative sequence.

Note that by weakening [Assumption 3.2](#) to the case where the total expectation over all realizations θ^k of the squared error is bounded, the theoretical results still hold; however, this condition is not practically verifiable.

The following assumption is crucial for establishing the convergence of [Algorithm 2.1](#) and for controlling the decay of the upper-level step size.

Assumption 3.3. The step size sequence $\{\alpha_k\}_{k=1}^\infty$ is non-increasing and positive, and satisfies:

- (i) $\sum_{k=1}^\infty \alpha_k^2 < \infty$ (square summability condition)
- (ii) $\lim_{k \rightarrow \infty} \frac{1}{k \alpha_k} = 0$ (step size decay condition)

These step size conditions are closely related to the classical Robbins–Monro criteria [41, 40] that ensure the convergence of stochastic approximation methods such as SGD. Condition (i), $\sum_{k=1}^\infty \alpha_k^2 < \infty$, is a standard requirement guaranteeing that the step sizes decrease sufficiently fast to suppress the variance of the stochastic gradients, thereby stabilizing the iterates. Condition (ii), $\lim_{k \rightarrow \infty} \frac{1}{k \alpha_k} = 0$, is a stronger requirement than the usual non-summability condition $\sum_{k=1}^\infty \alpha_k = \infty$. It enforces that α_k decays slower than $1/k$, a property often leveraged to establish optimal asymptotic convergence rates.

Lemma 3.4. [28, Proposition 2] **Expected Smoothness (ES):** Let [Assumption 3.1](#) hold, f is bounded below by f^{\inf} , and $\mathbb{E}[v_i^2] < \infty$ for $1 \leq i \leq m$. Then there exist constants $A, B, C \geq 0$ such that for all $\theta \in \mathbb{R}^d$, the stochastic gradient satisfies

$$\mathbb{E}_{v \sim \mathcal{D}}[\|\nabla f_v(\theta)\|^2] \leq 2A(f(\theta) - f^{\inf}) + B\|\nabla f(\theta)\|^2 + C.$$

The following auxiliary lemmas will be utilized in proving the convergence of inexact stochastic gradient.

Lemma 3.5. [46, Lemma 2] For all $\theta \in \mathbb{R}^d$, $v \sim \mathcal{D}$, and $\zeta > 0$ we have

$$(3.1) \quad |\langle \nabla f(\theta), \mathbb{E}_{v \sim \mathcal{D}}[e_v(\theta)] \rangle| \leq \frac{\|\nabla f(\theta)\|^2}{2\zeta} + \frac{\zeta}{2}(\mathbb{E}_{v \sim \mathcal{D}}[\|e_v(\theta)\|])^2$$

The following lemma relates the second moment of the inexact stochastic gradient with the stochastic gradient.

Lemma 3.6. [46, Lemma 3] *Let $\eta > 0$. The following relation between the second moment of the exact and inexact stochastic gradients hold*

$$(3.2) \quad \mathbb{E}_{v \sim \mathcal{D}} [\|z_v(\theta)\|^2] \leq \frac{1+\eta}{\eta} \mathbb{E}_{v \sim \mathcal{D}} [\|\nabla f_v(\theta)\|^2] + (1+\eta) \mathbb{E}_{v \sim \mathcal{D}} [\|e_v(\theta)\|^2].$$

Proposition 3.7. [46, Proposition 1] *Suppose Assumption 3.1 hold and $\mathbb{E}[v_i^2] < \infty$ for $1 \leq i \leq m$. Let $\eta > 0$, $\zeta > 0$, and $b(\zeta) = 1 - \frac{1}{2\zeta}$, $c(\zeta, \theta) = \frac{\zeta}{2} E^2(\theta)$, $\tilde{A}(\eta) = \frac{1+\eta}{\eta} A$, $\tilde{B}(\eta) = \frac{1+\eta}{\eta} B$, $\tilde{C}(\eta, \theta) = \frac{1+\eta}{\eta} C + (1+\eta) E^2(\theta)$. Then, for all $\theta \in \mathbb{R}^d$, the inexact stochastic gradient estimator satisfies*

$$(3.3) \quad \langle \nabla f(\theta), \mathbb{E}_{v \sim \mathcal{D}} [z_v(\theta)] \rangle \geq b(\zeta) \|\nabla f(\theta)\|^2 - c(\zeta, E^2(\theta)),$$

$$(3.4) \quad \mathbb{E}_{v \sim \mathcal{D}} [\|z_v(\theta)\|^2] \leq 2\tilde{A}(\eta)(f(\theta) - f^{\inf}) + \tilde{B}(\eta) \|\nabla f(\theta)\|^2 + \tilde{C}(\eta, E^2(\theta)).$$

The following lemma extends the ideas of [28, Lemma 2] and [41, Lemma 3.3] to the case that a biased inexact stochastic gradient (2.4) is employed. It plays a key role in proving the convergence of Algorithm 2.1.

Lemma 3.8. *Suppose Assumptions 3.1 and 3.2 hold, and z_k denote the approximate hypergradient defined in (2.3). Consider a non-increasing positive sequence of step sizes $\{\alpha_k\}_{k=0}^\infty$ with $\alpha_0 \leq \frac{\rho(2\zeta-1)}{\zeta L_{\nabla f} \tilde{B}}$, where $0 < \rho < 1$ and $\zeta > \frac{1}{2}$. Defining $\bar{\rho} := \frac{(1-\rho)(2\zeta-1)}{\zeta} > 0$ and $\mu := \gamma_1(1 + \alpha_0^2 L_{\nabla f} \tilde{A})$, we have*

$$\frac{\bar{\rho}}{2} \sum_{k=0}^{K-1} w_k r_k + \frac{w_{K-1}}{\alpha_{K-1}} \gamma_K \leq \frac{\mu}{\alpha_0} + \frac{(1+\eta)L_{\nabla f}}{2} \left(\frac{C}{\eta} \sum_{k=0}^{K-1} w_k \alpha_k + \sum_{k=0}^{K-1} \epsilon_k^2 w_k \alpha_k \right) + \frac{\zeta}{2} \sum_{k=0}^{K-1} \epsilon_k^2 w_k,$$

where $r_k := \mathbb{E} [\|\nabla f(\theta^k)\|^2]$, $w_0 := 1$ and $w_k := \frac{w_{k-1} \alpha_k}{\alpha_{k-1} (1 + L_{\nabla f} \alpha_k^2 \tilde{A})}$ for $k \geq 1$, and $\gamma_k := \mathbb{E}[f(\theta^k)] - f^{\inf}$.

Proof. Since f is $L_{\nabla f}$ -smooth, for all $k = 0, 1, \dots$ we have

$$\begin{aligned} f(\theta^{k+1}) &\leq f(\theta^k) + \langle \nabla f(\theta^k), \theta^{k+1} - \theta^k \rangle + \frac{L_{\nabla f}}{2} \|\theta^{k+1} - \theta^k\|^2 \\ &= f(\theta^k) + \alpha_k \langle \nabla f(\theta^k), -z_k \rangle + \frac{\alpha_k^2 L_{\nabla f}}{2} \|z_k\|^2. \end{aligned}$$

Taking conditional expectation over θ^k and utilizing Proposition 3.7 for bounding the term $\langle \nabla f(\theta^k), \mathbb{E}_{v^k \sim \mathcal{D}} [z_k] \rangle$ and $\mathbb{E}_{v^k \sim \mathcal{D}} [\|z_k\|^2]$, we have

$$\begin{aligned} \mathbb{E}[f(\theta^{k+1}) | \theta^k] &\leq f(\theta^k) - \alpha_k \langle \nabla f(\theta^k), \mathbb{E}_{v^k \sim \mathcal{D}} [z_k] \rangle + \frac{\alpha_k^2 L_{\nabla f}}{2} \mathbb{E}_{v^k \sim \mathcal{D}} [\|z_k\|^2] \\ &\stackrel{\text{Proposition 3.7}}{\leq} f(\theta^k) - \frac{2\zeta-1}{2\zeta} \alpha_k \|\nabla f(\theta^k)\|^2 + \frac{\zeta E_k^2}{2} \alpha_k \\ &\quad + \frac{\alpha_k^2 L_{\nabla f}}{2} (2\tilde{A}(f(\theta^k) - f^{\inf}) + \tilde{B} \|\nabla f(\theta^k)\|^2 + \tilde{C}), \end{aligned}$$

where $E_k^2 := \mathbb{E}_{v^k \sim \mathcal{D}}[e_{v^k}(\theta^k)^2]$. After simplification, we get

$$\begin{aligned} \mathbb{E}[f(\theta^{k+1})|\theta^k] &\leq f(\theta^k) + \alpha_k \left(\frac{\alpha_k L_{\nabla f} \tilde{B}}{2} - \frac{2\zeta - 1}{2\zeta} \right) \|\nabla f(\theta^k)\|^2 \\ &\quad + \alpha_k^2 L_{\nabla f} \tilde{A} (f(\theta^k) - f^{\inf}) + \frac{\alpha_k^2 L_{\nabla f}}{2} \left(\frac{1+\eta}{\eta} C + (1+\eta) E_k^2 \right) + \frac{\zeta E_k^2}{2} \alpha_k. \end{aligned}$$

Subtracting f^{\inf} from both sides, then using the tower property and rearranging, we get

$$\begin{aligned} \mathbb{E}[f(\theta^{k+1})] - f^{\inf} + \alpha_k \left(\frac{2\zeta - 1}{2\zeta} - \frac{\alpha_k L_{\nabla f} \tilde{B}}{2} \right) \mathbb{E}[\|\nabla f(\theta^k)\|^2] \\ \leq (1 + \alpha_k^2 L_{\nabla f} \tilde{A}) \mathbb{E}[f(\theta^k) - f^{\inf}] + \frac{\alpha_k^2 L_{\nabla f}}{2} \left(\frac{1+\eta}{\eta} C + (1+\eta) \mathbb{E}[E_k^2] \right) + \frac{\zeta \mathbb{E}[E_k^2]}{2} \alpha_k. \end{aligned}$$

Assumption 3.2 and the definition of the step size α_k yields

$$\frac{\bar{\rho}}{2} \alpha_k r_k \leq \gamma_k (1 + \alpha_k^2 L_{\nabla f} \tilde{A}) - \gamma_{k+1} + \frac{\alpha_k^2 L_{\nabla f}}{2} \left(\frac{1+\eta}{\eta} C + (1+\eta) \epsilon_k^2 \right) + \frac{\zeta \epsilon_k^2}{2} \alpha_k.$$

Multiplying both sides by $\frac{w_k}{\alpha_k}$, we get

$$\frac{\bar{\rho}}{2} w_k r_k \leq \frac{w_k (1 + \alpha_k^2 L_{\nabla f} \tilde{A})}{\alpha_k} \gamma_k - \frac{w_k}{\alpha_k} \gamma_{k+1} + \frac{\alpha_k L_{\nabla f}}{2} \left(\frac{1+\eta}{\eta} C + (1+\eta) \epsilon_k^2 \right) w_k + \frac{\zeta \epsilon_k^2}{2} w_k,$$

for all $k = 0, 1, \dots$. By definition of w_k , we have $\frac{w_k (1 + \alpha_k^2 L_{\nabla f} \tilde{A})}{\alpha_k} = \frac{w_{k-1}}{\alpha_{k-1}}$ for all $k \geq 1$. So, summing both sides for $k = 0, 1, \dots, K-1$, we have

$$\frac{\bar{\rho}}{2} \sum_{k=0}^{K-1} w_k r_k \leq \frac{\mu}{\alpha_0} - \frac{w_{K-1}}{\alpha_{K-1}} \gamma_K + \frac{(1+\eta) L_{\nabla f}}{2\eta} C \sum_{k=0}^{K-1} w_k \alpha_k + \frac{(1+\eta) L_{\nabla f}}{2} \sum_{k=0}^{K-1} \epsilon_k^2 w_k \alpha_k + \sum_{k=0}^{K-1} \frac{\zeta \epsilon_k^2}{2} w_k.$$

Rearranging yields the required result. \blacksquare

Theorem 3.9. *Let Assumptions 3.1 and 3.2 hold and the initial step size α_0 satisfies the bound in Lemma 3.8. Moreover, let μ , r_k , γ_k , and w_k be as defined in Lemma 3.8. We have*

$$\min_{0 \leq k \leq K-1} \mathbb{E}[\|\nabla f(\theta^k)\|^2] \leq \frac{1}{\bar{\rho} K w_K} \left(\frac{2\mu}{\alpha_0} + (1+\eta) L_{\nabla f} \left(\frac{C}{\eta} \sum_{k=0}^{K-1} w_k \alpha_k + \sum_{k=0}^{K-1} \epsilon_k^2 w_k \alpha_k \right) + \sum_{k=0}^{K-1} \zeta \epsilon_k^2 w_k \right).$$

Proof. Starting from Lemma 3.8, we have

$$\begin{aligned} \frac{\bar{\rho}}{2} \sum_{k=0}^{K-1} w_k r_k &\leq \frac{\bar{\rho}}{2} \sum_{k=0}^{K-1} w_k r_k + \frac{w_{K-1}}{\alpha_{K-1}} \gamma_K \\ &\leq \frac{\mu}{\alpha_0} + \frac{(1+\eta) L_{\nabla f}}{2} \left(\frac{C}{\eta} \sum_{k=0}^{K-1} w_k \alpha_k + \sum_{k=0}^{K-1} \epsilon_k^2 w_k \alpha_k \right) + \frac{\zeta}{2} \sum_{k=0}^{K-1} \epsilon_k^2 w_k. \end{aligned}$$

Dividing both sides by $W_K := \sum_{k=0}^{K-1} w_k$ yields

$$(3.5) \quad \frac{\bar{\rho}}{2W_K} \sum_{k=0}^{K-1} w_k r_k \leq \frac{\mu}{\alpha_0 W_K} - \frac{w_{K-1}}{\alpha_{K-1} W_K} \gamma_K + \frac{(1+\eta)L_{\nabla f}}{2W_K} \left(\frac{C}{\eta} \sum_{k=0}^{K-1} w_k \alpha_k + \sum_{k=0}^{K-1} \epsilon_k^2 w_k \alpha_k \right) + \frac{\zeta}{2W_K} \sum_{k=0}^{K-1} w_k \epsilon_k^2.$$

In order to simplify, since $W_K, \gamma_K, \alpha_{K-1}$ and all w_k are non-negative, we know

$$(3.6) \quad \frac{\bar{\rho}}{2} \left(\min_{0 \leq k \leq K-1} r_k \right) = \frac{\bar{\rho}}{2W_K} \left(\min_{0 \leq k \leq K-1} r_k \right) \sum_{k=0}^{K-1} w_k \leq \frac{\bar{\rho}}{2W_K} \sum_{k=0}^{K-1} w_k r_k + \frac{w_{K-1}}{\alpha_{K-1} W_K} \gamma_K.$$

Utilizing (3.6) in (3.5) yields

$$(3.7) \quad \frac{\bar{\rho}}{2} \left(\min_{0 \leq k \leq K-1} r_k \right) \leq \frac{\mu}{\alpha_0 W_K} + \frac{(1+\eta)L_{\nabla f}}{2W_K} \left(\frac{C}{\eta} \sum_{k=0}^{K-1} w_k \alpha_k + \sum_{k=0}^{K-1} \epsilon_k^2 w_k \alpha_k \right) + \frac{\zeta}{2W_K} \sum_{k=0}^{K-1} w_k \epsilon_k^2.$$

Since $\{\alpha_k\}_{k=0}^{\infty}$ is non-increasing, we have $\frac{\alpha_k}{\alpha_{k-1}} \leq 1$. Moreover, $\frac{1}{1+L_{\nabla f} \tilde{A} \alpha_k^2} \leq 1$. Hence,

$$w_k = w_{k-1} \left(\frac{\alpha_k}{\alpha_{k-1}} \right) \left(\frac{1}{1+L_{\nabla f} \tilde{A} \alpha_k^2} \right) \leq w_{k-1},$$

for all $k \geq 1$. Utilizing the inequality above together with the definition of W_K , we find

$$(3.8) \quad \frac{1}{W_K} = \frac{1}{\sum_{k=0}^{K-1} w_k} \leq \frac{1}{\sum_{k=0}^{K-1} \min_{0 \leq k \leq K-1} w_k} = \frac{1}{K w_K}$$

Using (3.8) in (3.7) and multiplying by $\frac{2}{\bar{\rho}}$ gives us the desired result. \blacksquare

Theorem 3.10. *Let Assumptions 3.1, 3.2, 3.3, and the bound on the initial step size as defined in Lemma 3.8 hold. Then there exists constants $C_1, C_2 > 0$ such that*

$$(3.9) \quad \min_{0 \leq k \leq K-1} \mathbb{E} [\|\nabla f(\theta^k)\|^2] \leq \frac{C_1}{K \alpha_K} + C_2 L_K,$$

where $L_K := \frac{1}{K \alpha_K} \sum_{k=0}^{K-1} \alpha_k \epsilon_k^2$. Moreover, if $\lim_{K \rightarrow \infty} L_K = 0$, then

$$\lim_{K \rightarrow \infty} \left(\min_{0 \leq k \leq K-1} \mathbb{E} [\|\nabla f(\theta^k)\|] \right) = 0.$$

Proof. Starting from Theorem 3.9 we can write

$$(3.10) \quad \min_{0 \leq k \leq K-1} r_k \leq \frac{1}{\bar{\rho}} \left(\frac{2\mu}{K \alpha_0 w_K} + \frac{(1+\eta)L_{\nabla f}}{K w_K} \left(\frac{C}{\eta} \sum_{k=0}^{K-1} w_k \alpha_k + \sum_{k=0}^{K-1} \epsilon_k^2 w_k \alpha_k \right) + \frac{\zeta}{K w_K} \sum_{k=0}^{K-1} \epsilon_k^2 w_k \right).$$

By definition of the weighting sequence we have

$$(3.11) \quad w_k = \frac{\alpha_k}{\alpha_0} \prod_{j=1}^k \frac{1}{1 + L_{\nabla f} \tilde{A} \alpha_j^2},$$

with the convention $\prod_{j=1}^0 c_j := 1$. Recall that, for a sequence of positive real numbers $\{y_j\}_{j \in \mathbb{N}}$, $\prod_{k=0}^{\infty} y_k$ converges to a finite value if and only if $\sum_{k=0}^{\infty} \log(y_k)$ converges to a finite value. Let $Q := \sum_{k=0}^{\infty} \alpha_k^2$, and so $Q < \infty$ by [Assumption 3.3\(i\)](#). For $y > -1$, we know $\log(1 + y) \leq y$, therefore

$$\sum_{k=1}^{\infty} \log(1 + L_{\nabla f} \tilde{A} \alpha_k^2) \leq \sum_{k=1}^{\infty} L_{\nabla f} \tilde{A} \alpha_k^2 \leq L_{\nabla f} \tilde{A} Q.$$

It implies that $P := \prod_{k=0}^{\infty} (1 + L_{\nabla f} \tilde{A} \alpha_k^2) < \infty$. Using the definition of P and (3.11), we have

$$(3.12) \quad \frac{1}{K w_K} = \frac{\alpha_0}{K \alpha_K} \prod_{j=1}^k \frac{1}{L_{\nabla f} \tilde{A} \alpha_j^2} \leq \frac{\alpha_0 P}{K \alpha_K}.$$

Moreover, we know

$$(3.13) \quad \sum_{k=0}^{K-1} w_k \alpha_k \leq \sum_{k=0}^{\infty} \frac{\alpha_k^2}{\alpha_0} \prod_{j=1}^k \frac{1}{1 + L_{\nabla f} \tilde{A} \alpha_j^2} \leq \frac{1}{\alpha_0} \sum_{k=0}^{\infty} \alpha_k^2 = \frac{Q}{\alpha_0} < \infty.$$

For the term $\sum_{k=0}^{K-1} \epsilon_k^2 w_k$, from (3.11) one can write

$$(3.14) \quad \sum_{k=0}^{K-1} \epsilon_k^2 w_k = \frac{1}{\alpha_0} \sum_{k=0}^{K-1} \alpha_k \epsilon_k^2 \prod_{j=1}^k \frac{1}{1 + L_{\nabla f} \tilde{A} \alpha_j^2} \leq \frac{1}{\alpha_0} \sum_{k=0}^{K-1} \alpha_k \epsilon_k^2.$$

Lastly, for the term $\sum_{k=0}^{K-1} \epsilon_k^2 w_k \alpha_k$, since $\alpha_k \leq \alpha_0$, we find

$$(3.15) \quad \sum_{k=0}^{K-1} \epsilon_k^2 w_k \alpha_k \leq \sum_{k=0}^{K-1} \alpha_k \epsilon_k^2 \prod_{j=1}^k \frac{1}{1 + L_{\nabla f} \tilde{A} \alpha_j^2} \leq \sum_{k=0}^{K-1} \alpha_k \epsilon_k^2.$$

Utilizing (3.13), (3.14), and (3.15) on the right-hand side of (3.10), we find

$$(3.16) \quad \min_{0 \leq k \leq K-1} r_k \leq \frac{1}{\bar{\rho}} \left(\frac{2\gamma_1(1 + \alpha_0^2 L_{\nabla f} \tilde{A})P}{K \alpha_K} + \frac{(1 + \eta)L_{\nabla f} \alpha_0 P}{K \alpha_K} \left(\frac{CQ}{\eta \alpha_0} + \sum_{k=0}^{K-1} \alpha_k \epsilon_k^2 \right) + \frac{\zeta P}{K \alpha_K} \sum_{k=0}^{K-1} \alpha_k \epsilon_k^2 \right),$$

which gives (3.9). Using [Assumption 3.3\(ii\)](#) and Jensen's inequality

$$\mathbb{E}[\|\nabla f(\theta^k)\|]^2 \leq \mathbb{E}[\|\nabla f(\theta^k)\|^2] = r_k,$$

we conclude the second result. ■

3.1. Examples of decay regimes with corresponding convergence rates. In this section, we provide a comprehensive theoretical analysis of the convergence properties of our algorithm. We establish convergence rates under different decay assumptions for the step size sequence $\{\alpha_k\}_{k=0}^\infty$ and approximation error sequence $\{\epsilon_k\}_{k=0}^\infty$.

Throughout our analysis, following the assumptions of [Theorem 3.10](#), we consider sequences $\{\alpha_k\}_{k=0}^\infty$ and $\{\epsilon_k\}_{k=0}^\infty$ satisfying the standard step size conditions in [Assumption 3.3](#). Our main theoretical objective is to ensure that $\lim_{K \rightarrow \infty} L_K = 0$, as per [Theorem 3.10](#).

We analyze distinct scenarios based on the decay rates of $\{\alpha_k\}_{k=0}^\infty$ and $\{\epsilon_k\}_{k=0}^\infty$.

3.1.1. Polynomial Decay for Step size and Accuracy Sequences.

Proposition 3.11. *Let $\alpha_k = O(k^{-q})$ with $\frac{1}{2} < q < 1$ and $\epsilon_k = O(k^{-p})$ for some $p > 0$. Then, for K large enough, considering L_K as defined in [Theorem 3.10](#), we have*

$$L_K = \begin{cases} O(K^{-\min\{2p, 1-q\}}), & q + 2p \neq 1, \\ O\left(\frac{\log K}{K^{1-q}}\right), & q + 2p = 1. \end{cases}$$

In particular, $\lim_{K \rightarrow \infty} L_K = 0$ for every $p > 0$ and $\frac{1}{2} < q < 1$.

Proof. By the assumptions, there exist constants $C > 0$ and $K_0 \in \mathbb{N}$ such that for all $k \geq K_0$

$$\alpha_k \epsilon_k^2 \leq C k^{-(q+2p)}.$$

Hence for $K \geq K_0$,

$$\sum_{k=K_0}^{K-1} \alpha_k \epsilon_k^2 \leq C \sum_{k=K_0}^{K-1} k^{-(q+2p)}.$$

Apply the integral-comparison bounds

$$\int_{K_0}^{K-1} t^{-(q+2p)} dt \leq \sum_{k=K_0}^{K-1} k^{-(q+2p)} \leq 1 + \int_{K_0}^{K-1} t^{-(q+2p)} dt,$$

and consider three cases.

Case 1: $q + 2p > 1$. The integral (and series) converges, so

$$\sum_{k=K_0}^{K-1} \alpha_k \epsilon_k^2 = O(1).$$

Using the assumption $\alpha_K = O(K^{-q})$ we have $K\alpha_K = O(K^{1-q})$, hence

$$L_K = \frac{1}{K\alpha_K} \left(\sum_{k=0}^{K_0-1} \alpha_k \epsilon_k^2 + \sum_{k=K_0}^{K-1} \alpha_k \epsilon_k^2 \right) = O(K^{-(1-q)}),$$

and therefore $\lim_{K \rightarrow \infty} L_K = 0$.

Case 2: $q + 2p = 1$. Then

$$\sum_{k=K_0}^{K-1} \alpha_k \epsilon_k^2 = \sum_{k=K_0}^{K-1} k^{-(q+2p)} = O(\log K),$$

and therefore

$$L_K = O\left(\frac{\log K}{K\alpha_K}\right) = O\left(\frac{\log K}{K^{1-q}}\right).$$

Since $1 - q > 0$ we conclude $\lim_{K \rightarrow \infty} L_K = 0$.

Case 3: $q + 2p < 1$. The integral behaves like $K^{1-(q+2p)}$, so

$$\sum_{k=K_0}^{K-1} \alpha_k \epsilon_k^2 = \sum_{k=K_0}^{K-1} k^{-(q+2p)} = O(K^{1-(q+2p)}),$$

Dividing by $K\alpha_K = O(K^{1-q})$ gives

$$L_K = O\left(\frac{K^{1-(q+2p)}}{K^{1-q}}\right) = O(K^{-2p}),$$

and thus $\lim_{K \rightarrow \infty} L_K = 0$.

Collecting the three cases combined with the fact that $\frac{1}{2} < q < 1$ yields the claimed piecewise estimates. \blacksquare

3.1.2. Polynomial Decay for $\{\alpha_k\}_{k=0}^{\infty}$ and Logarithmic Decay for $\{\epsilon_k\}_{k=0}^{\infty}$.

Proposition 3.12. *Let $\alpha_k = O(k^{-q})$ with $\frac{1}{2} < q < 1$ and $\epsilon_k = (\log k)^{-p}$ for $k \geq 2$ and some $p > 0$. Then, for K large enough,*

$$= O((\log K)^{-2p}).L_K = O((\log K)^{-2p}).$$

Consequently $\lim_{K \rightarrow \infty} L_K = 0$ for every $p > 0$.

Proof. Let $K_0 \geq 2$ be such that for all $k \geq K_0$ we have

$$\alpha_k \epsilon_k^2 \leq C_0 k^{-q} (\log k)^{-2p}$$

for some constant $C_0 > 0$. It suffices to bound

$$S_K := \sum_{k=K_0}^{K-1} k^{-q} (\log k)^{-2p},$$

since $\sum_{k=2}^{K-1} \alpha_k \epsilon_k^2 \leq C_0 S_K$ for $K \geq K_0$.

By the integral comparison test,

$$\int_{K_0}^{K-1} t^{-q} (\log t)^{-2p} dt \leq S_K \leq 1 + \int_{K_0}^{K-1} t^{-q} (\log t)^{-2p} dt.$$

Hence it is enough to show

$$I(K) := \int_{K_0}^{K-1} t^{-q} (\log t)^{-2p} dt = O(K^{1-q} (\log K)^{-2p}).$$

Perform the substitution $u = \log t$ (so $t = e^u$, $dt = e^u du$). Then

$$I(K) = \int_{\log K_0}^{\log(K-1)} e^{(1-q)u} u^{-2p} du.$$

Set $V := (1-q) \log(K-1)$ and $a := (1-q) \log K_0$ and change variable $v = (1-q)u$ (so $dv = (1-q)du$). This yields

$$I(K) = (1-q)^{-(1-2p)} \int_a^V e^v v^{-2p} dv.$$

Write

$$J(V) := \int_a^V e^v v^{-2p} dv.$$

Integrate by parts once with $g(v) = v^{-2p}$ and $h'(v) = e^v$ to obtain

$$J(V) = e^V V^{-2p} - e^a a^{-2p} + 2p \int_a^V e^v v^{-2p-1} dv.$$

For V large enough we have $v^{-2p-1} \leq V^{-1} v^{-2p}$ for all $v \in [a, V]$. Hence

$$\int_a^V e^v v^{-2p-1} dv \leq V^{-1} \int_a^V e^v v^{-2p} dv = V^{-1} J(V).$$

Combining with the integration-by-parts identity yields, for large V ,

$$J(V) \leq e^V V^{-2p} + C_a + 2pV^{-1}J(V),$$

where $C_a := e^a a^{-2p}$ is a fixed constant. Rearranging gives

$$(1 - 2pV^{-1})J(V) \leq e^V V^{-2p} + C_a.$$

Choose V_0 sufficiently large so that $1 - 2pV^{-1} \geq \frac{1}{2}$ for all $V \geq V_0$. For such V ,

$$J(V) \leq 2(e^V V^{-2p} + C_a) \leq C_1 e^V V^{-2p}$$

for some constant $C_1 > 0$. Tracing back the substitutions, we obtain for large K

$$I(K) = (1-q)^{-(1-2p)} J(V) \leq C_2 K^{1-q} (\log(K-1))^{-2p}$$

for some constant $C_2 > 0$. Therefore

$$S_K = O(K^{1-q} (\log K)^{-2p}).$$

Finally, since $\alpha_K = O(K^{-q})$ we have $K\alpha_K = O(K^{1-q})$, and hence

$$L_K = \frac{1}{K\alpha_K} (\alpha_0 \epsilon_0^2 + \alpha_1 \epsilon_1^2 + \sum_{k=2}^K \alpha_k \epsilon_k^2) \leq \frac{\alpha_0 \epsilon_0^2 + \alpha_1 \epsilon_1^2 + C_0 S_K}{K\alpha_K} = O((\log K)^{-2p}).$$

As $p > 0$ this implies $\lim_{K \rightarrow \infty} L_K = 0$, completing the proof. ■

Now, we can establish the rate of convergence with different options for accuracy and step size.

Corollary 3.13. *Let Assumptions 3.1, 3.2, and 3.3 hold and a suitable initial step size $\alpha_0 > 0$ is chosen as guided by Lemma 3.8.*

1. **Polynomial step size and polynomial error.** *If $\alpha_k = O(k^{-q})$ for $\frac{1}{2} < q < 1$ and $\epsilon_k = O(k^{-p})$ for $p > 0$, then*

$$(3.17) \quad \min_{0 \leq k \leq K-1} \mathbb{E}[\|\nabla f(\theta^k)\|] = \begin{cases} O(K^{-\min\{2p, 1-q\}/2}), & q + 2p \neq 1, \\ O\left(\sqrt{\frac{\log K}{K^{1-q}}}\right), & q + 2p = 1. \end{cases}$$

2. **Polynomial step size and logarithmic error.** *If $\alpha_k = O(k^{-q})$ for $\frac{1}{2} < q < 1$ and $\epsilon_k = O((\log k)^{-p})$ for $p > 0$, then*

$$(3.18) \quad \min_{0 \leq k \leq K-1} \mathbb{E}[\|\nabla f(\theta^k)\|] = O((\log K)^{-p}).$$

Proof. From Theorem 3.10 and Assumption 3.3(ii) we have

$$\min_{0 \leq k \leq K-1} \mathbb{E}\|\nabla f(\theta^k)\|^2 = O(L_K).$$

Now utilizing Jensen's inequality, Proposition 3.11 and Proposition 3.12, we conclude the required result. \blacksquare

Interpretation and guideline for parameter choice..

- If $2p < 1 - q$ the hypergradient accuracy limits the convergence and the gradient-rate is $O(k^{-p})$.
- If $2p > 1 - q$ the step size decay limits the convergence and the gradient-rate is $O(k^{-(1-q)/2})$.
- On the boundary $2p = 1 - q$ a logarithmic factor appears: the gradient-rate is $O(\sqrt{\log k}/k^{1-q})$.
- The best asymptotic rate achievable within these families is $O(k^{-1/4})$, obtained by taking $p \geq 1/4$ and letting $q \downarrow 1/2$ (i.e., choose q arbitrarily close to $1/2$ from above and $p \geq 1/4$).

Summary of rates. A comparison of convergence rates under different accuracy (polynomial and logarithmic) and step size (polynomial) schedules is presented in Table 1. Note that, as one can see in Table 1, even in cases where the rate does not depend on the accuracy schedule exponent p , its choice remains crucial in practice. In particular, we are interested in making p as small as possible, since it directly affects the computational cost.

4. Numerical experiments. Throughout our numerical experiments, based on Corollary 3.13, we select accuracy decay exponents $p \in \{0, 0.25, 0.5, 1, 2\}$ and step size decay exponents $q \in \{0, 0.5, 1\}$. The theoretically optimal choice is $(p, q) = (0.25, 0.5)$, which achieves the best convergence rate of $O(k^{-1/4})$. Note that $q = 0$ (fixed step size) only guarantees convergence to a neighborhood of the solution rather than exact convergence [46], though we include it to assess practical performance under finite computational budgets.

Step size α_k	Accuracy ϵ_k	Gradient rate	Note
	$O(k^{-p})$, $2p < 1 - q$	$O(k^{-p})$	limited by accuracy
$O(k^{-q})$, $\frac{1}{2} < q < 1$	$O(k^{-p})$, $2p = 1 - q$	$O(\sqrt{\frac{\log k}{k^{1-q}}})$	boundary: slower with $\log k$
	$O(k^{-p})$, $2p > 1 - q$	$O(k^{-(1-q)/2})$	limited by step size
	$O((\log k)^{-p})$	$O((\log k)^{-p})$	any $p > 0$; slowest

Table 1: Convergence rates for different step size and accuracy decay regimes.

Across all experiments, we use Nonmonotone Accelerated Proximal Gradient Descent (nmAPG) [31] to solve the lower-level problems. Since the lower-level objectives are smooth, we replace the proximal updates with standard gradient steps. Moreover, we use the Conjugate Gradient (CG) method to approximate the inverse Hessian of the lower-level objective through matrix–vector products computed via its corresponding linear system.

All of the codes are available on the GitHub repository¹ ([The repository will be made public upon acceptance of this manuscript](https://github.com/MohammadSadeghSalehi/Inexact_stochastic_bilevel_learning/)). Moreover, parts of the code and the general structure for computing hypergradients are adapted from [26]².

4.1. Denoising with Convex Ridge Regularizer. In this section, we perform image denoising task on colored images from the BSDS500 dataset [2]. Each image is augmented (by random and potentially overlapping crops) to 64×64 pixels. We consider 128 images in mini-batches of size 8 for training, and 16 images of size 192×192 (cropped to the center) as the test set. We then learn the parameters of a Convex Ridge Regularizer (CRR) [21] regularizer by solving the following bilevel optimization problem:

$$(4.1a) \quad \min_{\theta} \frac{1}{m} \sum_{i=1}^m \|\hat{x}_i(\theta) - x_i^*\|_2^2,$$

$$(4.1b) \quad \text{s.t. } \hat{x}_i(\theta) := \arg \min_{x \in \mathbb{R}^n} \{\|x - y_i\|_2^2 + R_\theta(x)\}, \quad i = 1, 2, \dots, m,$$

where x_i^* denotes the ground truth image, and y_i is the corresponding noisy observation corrupted by additive Gaussian noise: $y_i = x_i^* + \eta_i$, $\eta_i \sim \mathcal{N}(0, \sigma^2 I)$, $\sigma = 25/255$.

As a data-adaptive choice for the regularizer $R_\theta(x)$ in imaging problems, the Field of Experts (FoE) architecture [43, 8] is implemented as a composition of convolutional layers followed by smooth, convex potential functions. Following the advancements of this architecture and the convention introduced in [21, 22], we consider the CRR defined as:

$$R_\theta(x) = \sum_{i=1}^C \sum_{j=1}^H \sum_{k=1}^W [\psi^\beta (\exp(s) \odot \mathcal{W}(x))]_{i,j,k},$$

¹https://github.com/MohammadSadeghSalehi/Inexact_stochastic_bilevel_learning/

²<https://github.com/johertrich/LearnedRegularizers>

where \mathcal{W} is a multi-layer convolution operator composed of multiple convolution layers, $\psi^\beta: \mathbb{R} \rightarrow \mathbb{R}^+$ is a smooth convex potential, s is a learnable scaling parameter, \odot denotes the element-wise product, and C, H, W represent the channels (1 for grayscale and 3 for colored images), height, and width of images, respectively.

The convolution operator \mathcal{W} is composed of three zero-padded convolutional layers with kernel sizes 5×5 , increasing the number of output channels as $4 \rightarrow 8 \rightarrow 64$. Each convolutional kernel is reparametrized to have zero mean and is initialized using zero mean Xavier normal initialization. To ensure scale-invariance and stability, the composite convolutional operator is normalized via an estimate of its Lipschitz constant computed either using power iterations or in the Fourier domain. The resulting operator is further constrained to unit spectral norm using spectral normalization [22].

The potential function ψ^β is shared across all filters and scaled via the learnable factor α_j to obtain individual channel-wise potentials. Two convex choices for ψ^β include:

- The Huber function (Moreau envelope of the ℓ_1 -norm):

$$\psi^\beta(u) = \begin{cases} |u| - \frac{1}{2\beta}, & |u| > \frac{1}{\beta}, \\ \frac{\beta}{2}u^2, & |u| \leq \frac{1}{\beta}, \end{cases}$$

- The log-cosh function:

$$\psi^\beta(u) = \frac{1}{\beta} \log(\cosh(\beta u)).$$

These functions ensure convexity of ψ^β , and therefore of R_θ .

The gradient of R_θ with respect to x is computed via the chain rule:

$$\nabla R_\theta(x) = \mathcal{W}^\top [\psi'^\beta(\exp(s) \odot \mathcal{W}(x))] \odot \exp(s),$$

where \mathcal{W}^\top denotes the adjoint (transpose) of the convolution operator, implemented as a sequence of transposed convolutions with shared filters, and \odot denotes the element-wise (Hadamard) product. This regularizer is compatible with our required regularity assumptions on the lower-level problem.

In this experiment, we vary the initial accuracies $\epsilon_0 \in \{10^0, 10^{-2}, 10^{-4}\}$, initial step sizes $\alpha_0 \in \{10^{-2}, 10^{-3}\}$, and the exponents for the accuracy (k^{-p}) and step size schedules (k^{-q}), $p \in \{0, 0.25, 0.5, 1, 2\}$ and $q \in \{0, 0.5, 1\}$. We first compare the performance of ISGD for each initial accuracy separately, as shown in Figure 1. We display only configurations that achieved reasonable training performance in terms of training convergence behavior, filtering out divergent or severely suboptimal settings. Selected marginal or divergent configurations based on Theorem 3.10 and Corollary 3.13 are presented to justify the reasonableness of the chosen settings.

We evaluated performance based on two criteria: convergence speed under a limited computational budget and lower overall loss with more stable behavior throughout training, especially, at its final stages. We measure computational cost as the total number of lower-level solver iterations plus the linear system solver (used in computing the hypergradient) iterations. This measure captures the dominant sources of computational effort in bilevel optimization while remaining independent of implementation or hardware details [45]. We set a budget of

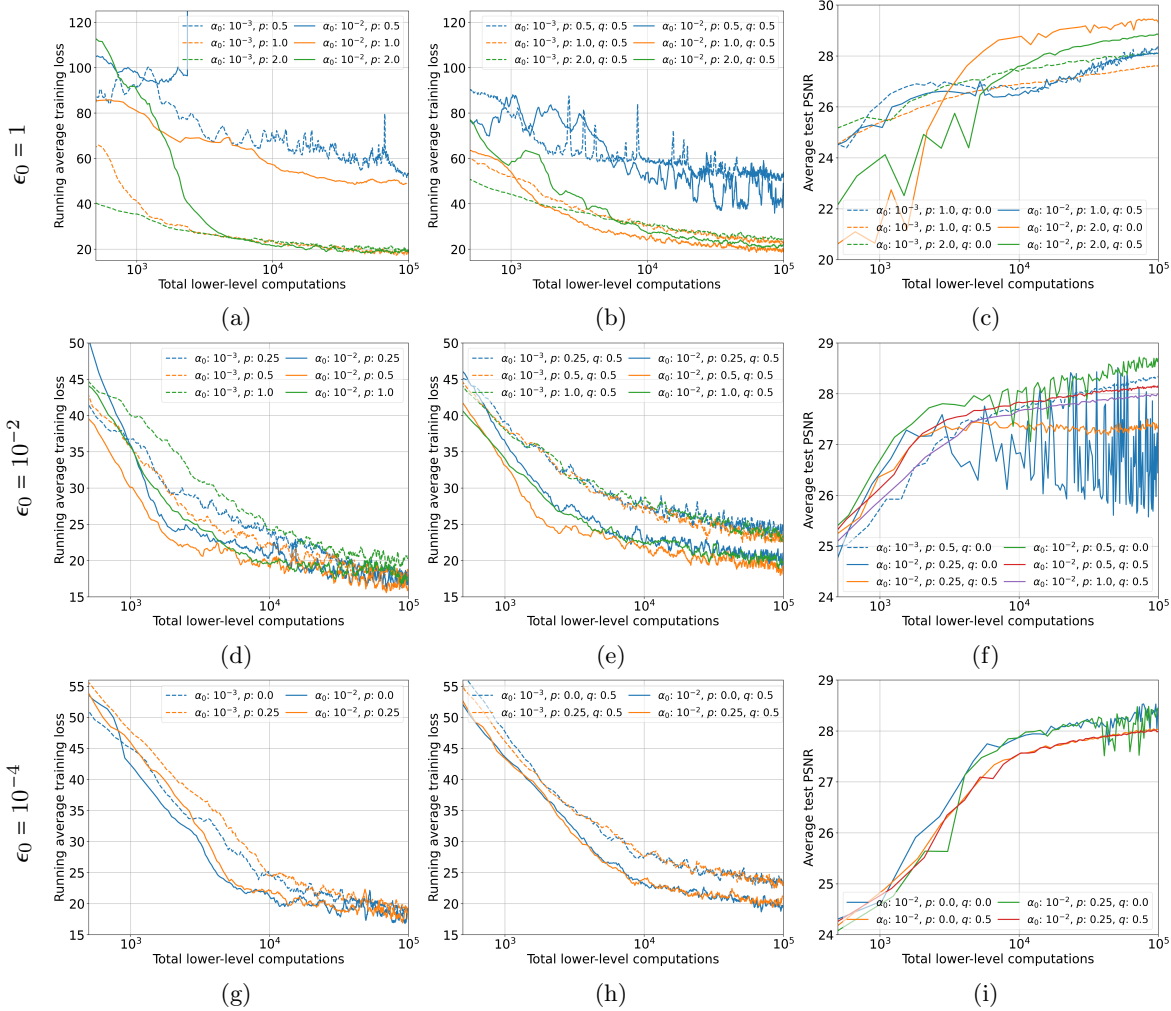


Figure 1: Training and test results for initial accuracies $\epsilon_0 = 1$, $\epsilon_0 = 10^{-2}$, $\epsilon_0 = 10^{-4}$. The first column (a), (d), (g) shows training loss with a fixed upper-level step size. The second column (b), (e), (h) represents training loss with a decreasing upper-level step size with decreasing schedule exponent $q > 0$. The last column (c), (f), (i) illustrates test PSNR comparison between the best-performing fixed and decreasing step size configurations.

10^5 total computational cost to ensure a fair comparison across experiments. The performance of different settings under these criteria is shown in Figure 1.

First, by starting from a large accuracy $\epsilon_0 = 1$, it can be seen in Figures 1a, 1b, and 1c that only aggressive accuracy decrease schedules such as k^{-1} and k^{-2} result in a meaningful reduction in loss values. As shown in Figure 1a, for this large initial tolerance and a fixed step size of $\alpha_0 = 10^{-3}$, the k^{-2} schedule initially yields a faster decrease in loss. However, the k^{-1} schedule catches up after slightly more than 10^3 computations. Initially slower, the

setting with a larger fixed step size 10^{-2} eventually joins the aforementioned curves, showing that with sufficient accuracy adjustment, it can be an effective step size.

While a large tolerance of $\epsilon_0 = 1$ combined with a fixed large step size of $\alpha_0 = 10^{-2}$ and any accuracy schedule less aggressive than k^{-2} tends to be suboptimal or even divergent, as shown in [Figure 1b](#), a modest step size decay such as $k^{-0.5}$ significantly improves performance, making it comparable to the fixed $\alpha_0 = 10^{-3}$, and stabilizes the training loss behavior. On the other hand, while decreasing step sizes starting from $\alpha_0 = 10^{-3}$ result in reduced variance initially, they slow down and yield higher loss values under the fixed budget compared to the same fixed step size.

Finally, the test PSNR results in [Figure 1c](#) show that while decreasing the step size reduces test-time variance, its benefits are most pronounced when combined with a larger initial step size ($\alpha_0 = 10^{-2}$). The best overall performance is achieved using a fixed step size of $\alpha_0 = 10^{-2}$. These results suggest that the choice of the accuracy schedule is more critical. Depending on the user's utility, decreasing the step size can prevent blowups in training, as it is visible in [Figures 1a](#) and [1c](#), but may lower performance under a finite computational budget. Even with a suitable accuracy, a fixed step size can result in oscillatory and suboptimal performance under a very limited budget. However, with a larger computational budget and validation monitoring, it can lead to better performance. Step size tuning can be performed using shorter runs, for example, by examining performance after 10^2 to 10^3 computations, as shown in [Figure 1a](#).

Starting with a mid-level accuracy of $\epsilon_0 = 10^{-2}$, a larger initial step size of $\alpha_0 = 10^{-2}$ performs better compared to the corresponding settings for $\epsilon_0 = 10^{-3}$, as shown in [Figures 1d](#) and [1e](#). In [Figure 1d](#), the accuracy decay rate $p = 1$ appears overly aggressive, while $p = 0.25$ is insufficient. The intermediate value $p = 0.5$ yields the best performance.

When the step size is decreased, as shown in [Figure 1e](#), training becomes more stable, variance is reduced, and the gap between settings with initial step sizes of 10^{-2} and 10^{-3} becomes more pronounced. However, the overall performance and the ranking of suitable accuracy decay schedules remain similar to those observed with a fixed step size, underscoring the importance of selecting an appropriate accuracy schedule. Interestingly, the setting $\alpha_0 = 10^{-2}, p = 0.25, q = 0.5$, while effective during training ([Figure 1e](#)) and provides optimal theoretical rate ([Corollary 3.13](#)), leads to suboptimal test performance. This is further supported by the test PSNR results in [Figure 1f](#), where a decreasing step size yields significantly lower variance, but the best performance under a fixed computational budget is achieved using a fixed step size combined with the appropriate accuracy schedule $k^{-0.5}$, reaching 0.5 dB PSNR improvement over the counterpart with decreasing step size.

Starting with a high accuracy level of $\epsilon_0 = 10^{-4}$, [Figures 1g](#), [1h](#), and [1i](#) show that, in a finite-time setting, decreasing the accuracy is less critical and may even slightly slow down performance due to more computations than necessary. A similar pattern to the mid-accuracy case is observed for the step size: the larger step size ($\alpha_0 = 10^{-2}$) yields the best performance even without any decay, while decreasing step size variants reduce variance but result in overall weaker fixed-budget outcomes (see [Figure 1i](#)).

However, this high-accuracy scenario is less attractive in practice, as it requires significant computational effort from the early stages of training, and what is sufficiently high accuracy for a given problem is not known a priori. From a practical perspective, it is ultimately up to the

user to choose between lower but more stable and predictable performance, with no test PSNR drop and stronger theoretical support, or higher peak performance at the cost of potential test-time drops and fluctuations. Note that validation and testing are computationally expensive in the bilevel setting, unlike in common machine learning tasks, as they require solving the lower-level problem with many iterations to achieve high-accuracy inference. Thus, one might want to avoid it while still ensuring that the method does not behave erratically, which encourages the use of a decreasing step size. As observed in Figures 1a and 1b, starting with a large ϵ_0 requires a sharp decay rate in accuracy. Moreover, as ϵ_0 decreases (for instance after 10^4 computations in Figures 1a and 1b), the decay rate should be less aggressive to yield the best results. A multi-level or adaptive strategy that begins with large ϵ_0 and chooses p to be as small as possible and as large as necessary, could potentially achieve a desirable performance with substantially fewer computations.

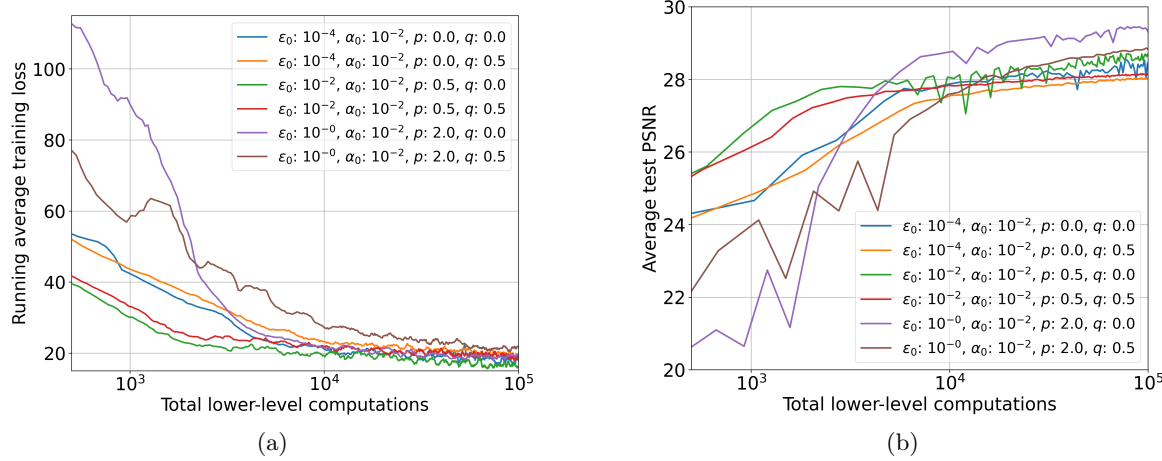


Figure 2: Best-performing fixed and decreasing step size configurations across all accuracy settings $\epsilon_0 \in \{10^0, 10^{-2}, 10^{-4}\}$. (a) Training loss plotted against computational cost. (b) Test PSNR plotted against computational cost.

By selecting the best-performing settings and plotting them together, as shown in Figure 2, it becomes clear that choosing an appropriate accuracy schedule based on the initial accuracy ϵ_0 , specifically, using a larger p for larger ϵ_0 , can yield desirable training and test performance. The mid-accuracy case $\epsilon_0 = 10^{-2}$ with decreasing accuracy performed best initially up to around 10^4 computations, and once finding a suitable accuracy, $\epsilon_0 = 1$ with $p = 2$ takes over, although this could not have been known a priori.

Furthermore, although our convergence theorem (Theorem 3.10) requires a decreasing step size with $0.5 < q < 1$, in practice a non-decreasing step size can yield better finite-budget performance, as shown in Figure 2. This suggests room for improved non-asymptotic analysis, while decreasing step sizes reduce training variance and produce more stable test results.

The qualitative results at selected testing checkpoints corresponding to different training settings are shown in Figure 3, and they align well with the performance curves in Figure 2.

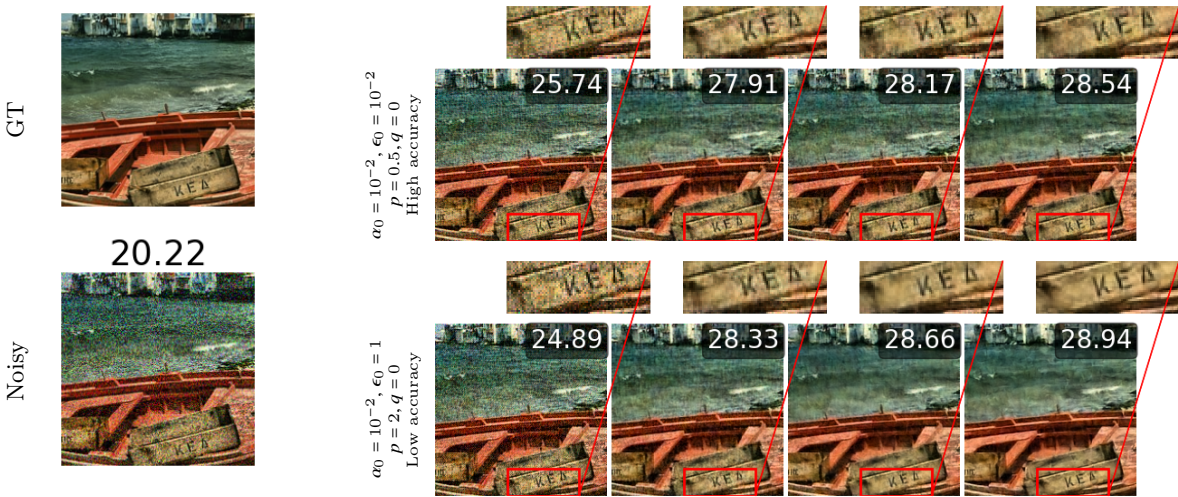


Figure 3: Denoising results on test data at training checkpoints corresponding to computational costs of 5,000; 10,000; 50,000; and 100,000. Each row displays outputs from different hyperparameter configurations.

The configuration with $\epsilon_0 = 1$ and $p = 2$ achieves the overall best performance, as evident in Figure 3. While the setting with $\epsilon_0 = 10^{-2}$ and $p = 0.5$ performs best in the early stages, it ultimately ranks second, though still outperforming the high-accuracy setting $\epsilon_0 = 10^{-4}$, which could not have been anticipated a priori. These results suggest that, by selecting an appropriate accuracy-decay schedule (independent of the initial accuracy) and using a fixed step size, one can reliably obtain a well-trained denoising prior.

4.2. Inpainting with Convex Ridge Regularizer.

Image Inpainting. To analyze our approach on a more complicated inverse problem (non-trivial forward operator), we consider an image inpainting task using grayscale images of size 96×96 . The training data consists of 128 randomly selected and cropped images of the BSDS500 dataset [2], where each image is corrupted by randomly masking 70% of the pixels using a Bernoulli mask $M_{ij} \sim \text{Bernoulli}(p)$, $1 \leq i, j \leq 96$, with $p = 0.3$, and the observation is given by $y = M \odot x$, which corresponds to retaining approximately 30% of the original data, implemented via the Bernoulli Splitting Mask Generator³. Additionally, additive Gaussian noise with standard deviation $\sigma = 0.02$ is applied to the unmasked pixels. This setting corresponds to solving the bilevel problem in (4.1), where the data fidelity term in the lower-level problem (1.1b) is modified to $\|Ax - y\|_2^2$, with A representing the inpainting (binary masking) operator and $y \in \mathbb{R}^{96 \times 96}$ the observed noisy and incomplete image. The regularizer $R_\theta(x)$ uses the same CRR architecture as in subsection 4.1, with the input channel changed to 1 to support grayscale images, and an additional penalty term $\frac{\xi}{2}\|x\|^2$ with $\xi = 10^{-6}$ to ensure strong convexity of the lower-level problem. The upper-level loss (1.1a) remains unchanged, with x_i^* denoting the full ground truth image. The same training and evaluation

³BernoulliSplittingMaskGenerator documentation

pipeline as in the denoising experiment is employed, with mini-batches and data augmentations appropriately adjusted for the new image size.

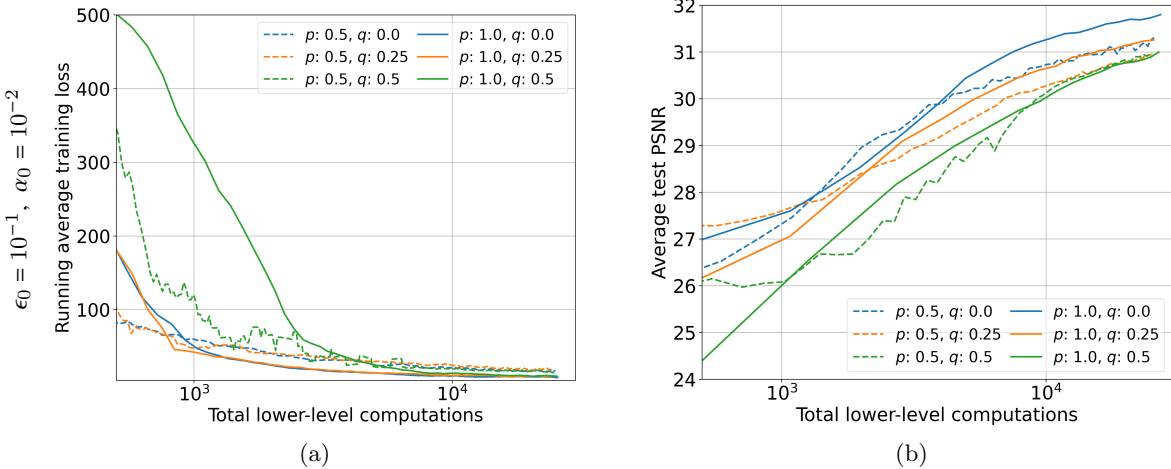


Figure 4: Running average training loss and average test PSNR for inpainting, plotted against total computational cost. Results are shown for upper-level step size $\alpha_0 = 10^{-2}$, initial accuracy $\epsilon_0 = 10^{-1}$, accuracy schedule exponent $p \in \{0.5, 1\}$, and step size decay exponent $q \in \{0, 0.25, 0.5\}$. All settings with $p = 1$ appear to perform faster than their $p = 0.5$ counterparts.

Considering a large initial accuracy of $\epsilon_0 = 10^{-1}$ and a large step size of $\alpha_0 = 10^{-2}$, chosen via grid search, together with accuracy and step size decay exponents $p \in \{0.5, 1\}$ and $q \in \{0, 0.25, 0.5\}$, the training and testing results for learning a CRR regularizer for image inpainting are shown in Figure 4. As illustrated in Figure 4(a), for both values of p , the fixed step size ($q = 0$) and the moderately decaying step size ($q = 0.25$) perform comparably during training, with the fixed-step variant achieving higher PSNR in testing. In contrast, the more aggressive decay $q = 0.5$ leads to slower training and lower test PSNR for both values of p . Although all settings converge to very similar training losses after an extensive computational cost of 10^4 , the configurations with $p = 0.5$ reach lower training loss faster than those with $p = 1$. However, beyond a computational cost of about 10^3 , the test PSNR of the $p = 1$ settings surpasses that of $p = 0.5$. The growth of testing PSNR in regions where the training loss exhibits low curvature reflects the complex relationship between optimization and generalization in machine learning. Similar to the denoising case, starting from a large initial accuracy, a fixed step size combined with a suitable accuracy-decay schedule can yield the best overall training and testing performance.

Given the results in Figure 4, when fixing $p = 1$ and checkpointing the test quality after specific training computational costs, one can observe that the fixed step size consistently outperforms the decreasing variants with $q \in \{0.25, 0.5\}$ throughout training, resulting in a clear PSNR advantage under the same computational budget as illustrated in Figure 5. This indicates that, by appropriately tuning the initial step size, one can obtain a desirable learned

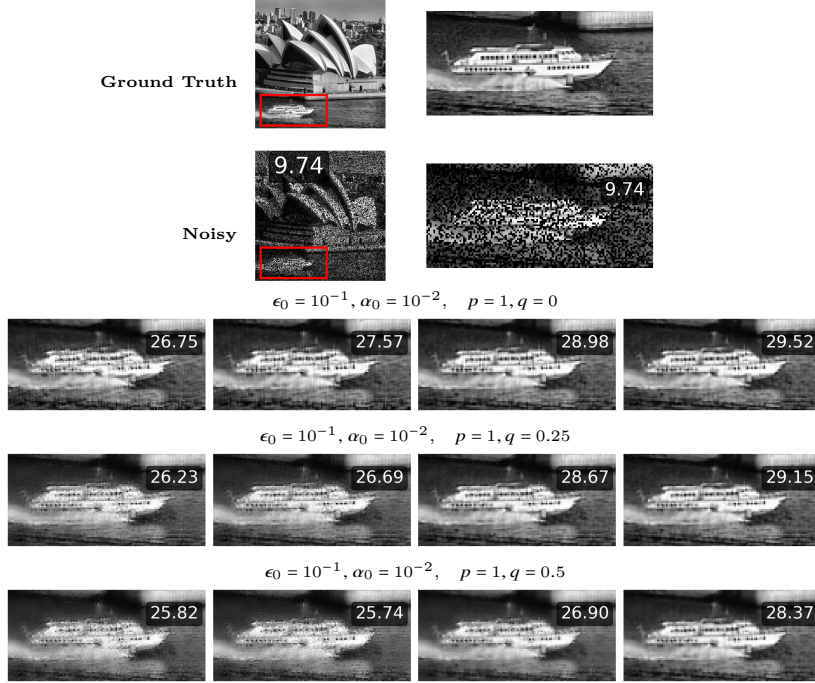


Figure 5: Inpainting comparison across different decreasing schedule exponent $q \in \{0, 0.25, 0.5\}$ configurations for fixed upper-level step size, initial accuracy, and accuracy decreasing schedule. Top: ground truth and noisy input image with the zoomed cropped region. Each row shows the zoomed cropped of output across training checkpoints corresponding to computational costs of 2,500; 5,000; 10,000; and 20,000, with the specified hyperparameters.

regularizer even with a fixed step size during training. With the more suitable choice of $p = 1$ in this experiment, the results show improved test stability for the decreasing step size variants. During training, however, $q = 0.5$ appears more aggressive than necessary under a fixed computational budget, while $q = 0.25$ performs slightly better than $q = 0$, particularly before 10^3 computations.

4.3. ISGD vs IAdam: Denoising with Input-Convex Neural Network Regularizer. In this experiment, we consider the input-convex neural network (ICNN) architecture [1, 34] as the regularizer $R_\theta(x)$ with 2 layers and the following form:

$$R_\theta(x) = \sum_{i=1}^C \sum_{j=1}^H \sum_{k=1}^W [\phi(W_z \phi(W_x x + b_x) + b_z) \odot \exp(s)]_{i,j,k},$$

where W_x and W_z denote 2D convolution operators, \odot is the element-wise product, and W_x , W_z , b_x , b_z , and s are trainable parameters. Note that W_z is constrained to be non-negative; we enforce this by clamping its negative weights to zero. Additionally, W_x is initialized with zero-mean filters to ensure improved performance.

The activation function $\phi : \mathbb{R} \rightarrow \mathbb{R}$ is a smoothed clipped ReLU defined as:

$$\phi(u) = \begin{cases} 0, & u < 0, \\ \frac{u^2}{2\nu}, & 0 \leq u < \nu, \\ u - \frac{\nu}{2}, & u \geq \nu, \end{cases}$$

where $\nu > 0$ is a small smoothing parameter. This architecture ensures convexity of the regularizer $R_\theta(x)$ with respect to x and satisfies the regularity assumptions required in our theoretical analysis. In our experiments, we set $\nu = 10^{-3}$.

[Figure 6](#) compares ISGD with IAdam, where IAdam refers to the Adam algorithm [30] with the inexact stochastic hypergradient replacing the exact stochastic hypergradient. The comparison spans low, medium, and high accuracies $\epsilon_0 \in \{1, 10^{-2}, 10^{-4}\}$ with an initial step size of $\alpha_0 = 10^{-2}$ and various decreasing accuracy and step size schedules.

Since ICNN parameters can vary significantly in magnitude, the optimization process may be affected by using the same step size across all of them. As shown in [Figure 6](#), preconditioning and diagonal rescaling in Adam provide clear advantages over SGD across all settings. [Figure 6a](#) further shows that, with a fixed step size, all IAdam variants converge to the same loss region after a computational cost of 10^4 . While the high-accuracy case $\epsilon_0 = 10^{-4}$ converges more slowly at first, the variants with $\epsilon_0 = 10^{-2}$ and $\epsilon_0 = 1$ exhibit similar behavior throughout. In contrast, ISGD variants with fixed step size display higher variance and perform worse than IAdam under the same computational budget.

On the other hand, introducing a decreasing step size, while not significantly affecting IAdam's performance, substantially stabilizes training and reduces the variance of ISGD variants, making them comparable to IAdam by the end of training, as shown in [Figure 6b](#). Selecting the two best settings of both methods, illustrated in [Figure 6c](#) and [Figure 6d](#), highlights how a decreasing step size can stabilize and improve both training and testing performance for ISGD, bringing it closer to IAdam. The robustness of IAdam variants and their superiority in terms of both training loss and test PSNR motivate the exploration of preconditioning techniques in future work.

It is worth noting that while a decreasing step size has only a minor effect on IAdam's training performance, it stabilizes the test results, as shown in [Figure 6d](#).

Considering the training checkpoints in [Figure 7](#), the importance of preconditioning and the superior performance of IAdam under a limited computational budget become even more evident. The substantial gap of more than 2 dB PSNR in the early phase of training, compared with ISGD, highlights the role of rescaling the hypergradient in accelerating convergence.

5. Conclusion and Future Work. In this work, we advanced the theoretical and practical analysis of inexact stochastic bilevel optimization, establishing explicit convergence rates under different accuracy and step size schedules, and validating these findings on large-scale imaging problems. Our analysis shows that while decaying step sizes are necessary for asymptotic guarantees, accuracy scheduling plays a more decisive role in practice, and preconditioned adaptive methods such as Adam can substantially enhance performance. Experiments across denoising and inpainting tasks confirm that theory-informed schedules improve stability, but also highlight that fixed or more aggressive schedules often deliver superior results under realistic computational budgets.

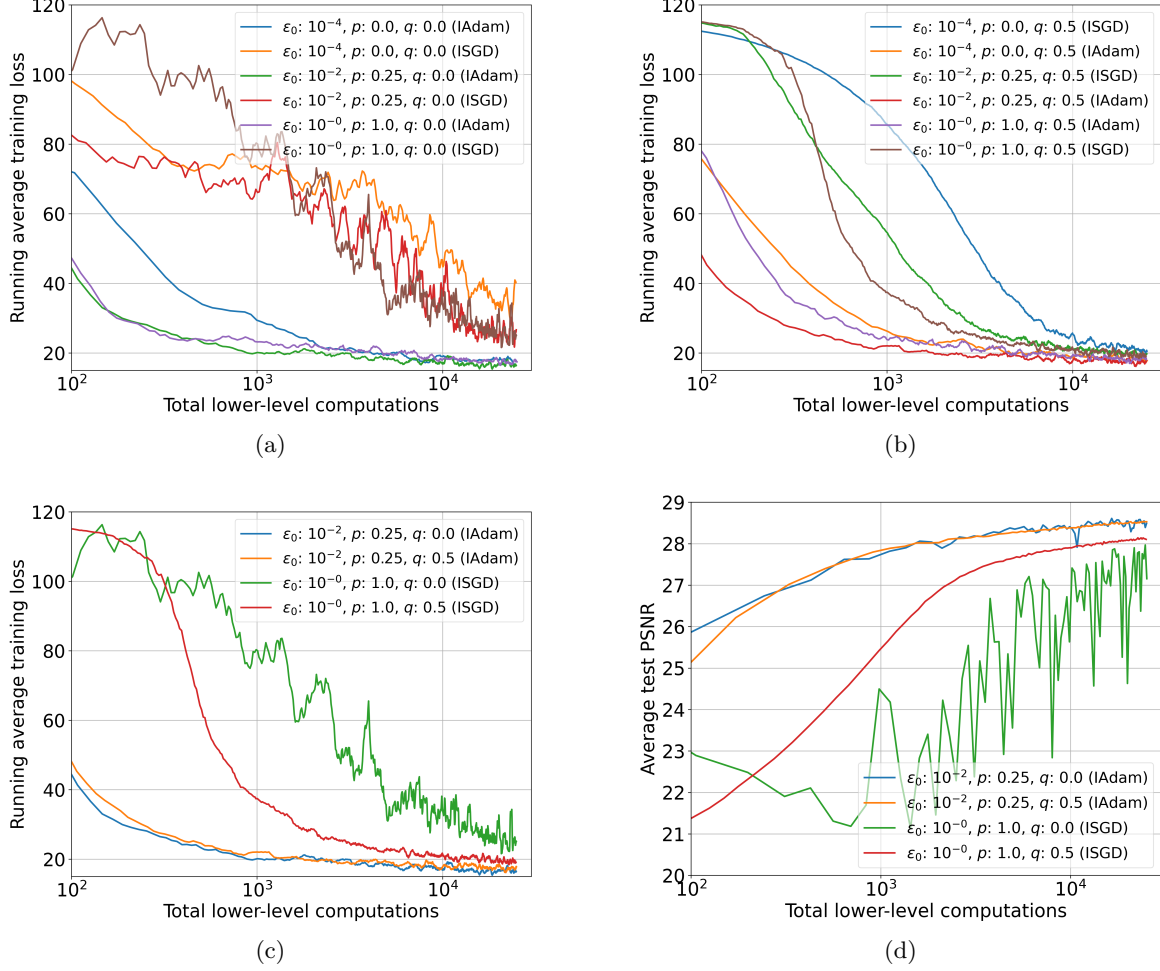


Figure 6: Comparison between SGD and Adam with inexact stochastic hypergradients across different initial accuracies, using the most suitable values of accuracy schedule exponent p and step size schedule exponent q for each, found by trial and error. Top row: (a) shows configurations with fixed step size; (b) corresponds to decreasing step size. Bottom row: best-performing configurations of ISGD and IAdam in terms of training loss and test PSNR in (c) and (d), respectively.

These results narrow the gap between convergence theory and applied bilevel learning, but also reveal a persistent mismatch between asymptotic guarantees and finite-budget performance. Bridging this gap presents exciting directions for future work. In particular, developing non-asymptotic convergence theory that captures finite-time behavior, designing adaptive accuracy and step size schedules guided by data and budget constraints, and extending our analysis to nonconvex lower-level problems remain key challenges.

By combining theoretical guarantees with practical insights, we take a step toward making



Figure 7: Denoising results for ICNN regularizer under various hyperparameter settings. First two rows corresponds to a best performed ISGD configuration, and the rest of the rows show the best top IAdam configuration.

bilevel optimization a more reliable and scalable tool for modern machine learning and large-scale challenges in inverse problems.

REFERENCES

- [1] B. AMOS, L. XU, AND J. Z. KOLTER, *Input convex neural networks*, in Proceedings of the 34th International Conference on Machine Learning, D. Precup and Y. W. Teh, eds., vol. 70 of Proceedings of Machine Learning Research, PMLR, 06–11 Aug 2017, pp. 146–155, <https://proceedings.mlr.press/v70/amos17b.html>.
- [2] P. ARBELAEZ, M. MAIRE, C. FOWLKES, AND J. MALIK, *Contour detection and hierarchical image segmentation*, IEEE Trans. Pattern Anal. Mach. Intell., 33 (2011), pp. 898–916, <https://doi.org/10.1109/TPAMI.2010.161>.
- [3] L. BOGENSPERGER, A. CHAMBOLLE, AND T. POCK, *Convergence of a piggyback-style method for the*

differentiation of solutions of standard saddle-point problems, SIAM Journal on Mathematics of Data Science, 4 (2022), pp. 1003–1030, <https://doi.org/10.1137/21M1455887>.

[4] L. BOGENSPERGER, M. J. EHRHARDT, T. POCK, M. S. SALEHI, AND H. S. WONG, *An Adaptively Inexact Method for Bilevel Learning Using Primal-Dual-Style Differentiation*, Journal of Mathematical Imaging and Vision, 67 (2025), p. 49, <https://doi.org/10.1007/s10851-025-01262-w>.

[5] J. BOLTE, E. PAUWELS, AND S. VAITER, *Automatic differentiation of nonsmooth iterative algorithms*, in Advances in Neural Information Processing Systems, S. Koyejo, S. Mohamed, A. Agarwal, D. Belgrave, K. Cho, and A. Oh, eds., vol. 35, Curran Associates, Inc., 2022, pp. 26404–26417.

[6] J. BOLTE, E. PAUWELS, AND S. VAITER, *One-step differentiation of iterative algorithms*, in Thirty-seventh Conference on Neural Information Processing Systems, 2023, <https://openreview.net/forum?id=81snFfE3vR>.

[7] T. A. BUBBA, M. SANTACESARIA, AND A. SEBASTIANI, *Tomoselfeq: Self-supervised deep equilibrium learning for sparse-angle ct reconstruction*, in Scale Space and Variational Methods in Computer Vision, T. A. Bubba, R. Gaburro, S. Gazzola, K. Papafitsoros, M. Pereyra, and C.-B. Schönlieb, eds., Cham, 2025, Springer Nature Switzerland, pp. 334–346.

[8] Y. CHEN, R. RANFTL, AND T. POCK, *Insights into analysis operator learning: From patch-based sparse models to higher order MRFs*, IEEE Transactions on Image Processing, 23 (2014), pp. 1060–1072.

[9] C. DANIELE, S. VILLA, S. VAITER, AND L. CALATRONI, *Deep equilibrium models for poisson imaging inverse problems via mirror descent*, 2025, <https://arxiv.org/abs/2507.11461>.

[10] L. DAVY, L. M. BRICENO-ARIAS, AND N. PUSTELNIK, *Restarted contractive operators to learn at equilibrium*, 2025, <https://arxiv.org/abs/2506.13239>.

[11] Y. DEMIDOVICH, G. MALINOVSKY, I. SOKOLOV, AND P. RICHTÁŘIK, *A guide through the zoo of biased SGD*, in Thirty-seventh Conference on Neural Information Processing Systems, 2023, <https://openreview.net/forum?id=OCtv4NyahI>.

[12] N. DIZON AND T. VALKONEN, *Differential estimates for fast first-order multilevel nonconvex optimisation*, 2025, <https://arxiv.org/abs/2412.01481>.

[13] S. DOWNING, S. GAZZOLA, I. G. GRAHAM, AND E. A. SPENCE, *Optimising seismic imaging design parameters via bilevel learning*, Inverse Problems, 40 (2024), p. 115008, <https://doi.org/10.1088/1361-6420/ad797a>.

[14] M. J. EHRHARDT, S. GAZZOLA, AND S. J. SCOTT, *Efficient gradient-based methods for bilevel learning via recycling krylov subspaces*, 2024, <https://arxiv.org/abs/2412.08264>.

[15] M. J. EHRHARDT AND L. ROBERTS, *Inexact derivative-free optimization for bilevel learning*, J. Math. Imaging Vis., 63 (2021), pp. 580–600.

[16] M. J. EHRHARDT AND L. ROBERTS, *Analyzing inexact hypergradients for bilevel learning*, IMA Journal of Applied Mathematics, 89 (2023), pp. 254–278, <https://doi.org/10.1093/imamat/hxad035>.

[17] H. FATHI, A. SKORIKOV, AND T. VAN LEEUWEN, *Bi-level optimization and implicit differentiation as a framework for optimal experimental design in tomography*, in Scale Space and Variational Methods in Computer Vision: 10th International Conference, SSVM 2025, Dartington, UK, May 18–22, 2025, Proceedings, Part II, Berlin, Heidelberg, 2025, Springer-Verlag, p. 123–135, https://doi.org/10.1007/978-3-031-92369-2_10.

[18] L. FRANCESCHI, M. DONINI, P. FRASCONI, AND M. PONTIL, *Forward and reverse gradient-based hyperparameter optimization*, in Proceedings of the 34th International Conference on Machine Learning, D. Precup and Y. W. Teh, eds., vol. 70 of Proceedings of Machine Learning Research, PMLR, 06–11 Aug 2017, pp. 1165–1173.

[19] S. W. FUNG, H. HEATON, Q. LI, D. MCKENZIE, S. OSHER, AND W. YIN, *Jfb: Jacobian-free backpropagation for implicit networks*, Proceedings of the AAAI Conference on Artificial Intelligence, 36 (2022), pp. 6648–6656, <https://doi.org/10.1609/aaai.v36i6.20619>.

[20] S. GHADIMI AND G. LAN, *Stochastic first- and zeroth-order methods for nonconvex stochastic programming*, SIAM Journal on Optimization, 23 (2013), pp. 2341–2368, <https://doi.org/10.1137/120880811>.

[21] A. GOUJON, S. NEUMAYER, P. BOHRA, S. DUCOTTERD, AND M. UNSER, *A neural-network-based convex regularizer for inverse problems*, IEEE Trans. Comput. Imaging, 9 (2023), pp. 781–795, <https://doi.org/10.1109/TCI.2023.3306100>.

[22] A. GOUJON, S. NEUMAYER, AND M. UNSER, *Learning weakly convex regularizers for convergent image-reconstruction algorithms*, SIAM J. Imaging Sci., 17 (2024), pp. 91–115.

[23] R. M. GOWER, N. LOIZOU, X. QIAN, A. SAILANBAYEV, E. SHULGIN, AND P. RICHTÁRIK, *SGD: General analysis and improved rates*, in Proceedings of the 36th International Conference on Machine Learning, K. Chaudhuri and R. Salakhutdinov, eds., vol. 97 of Proceedings of Machine Learning Research, PMLR, 09–15 Jun 2019, pp. 5200–5209, <https://proceedings.mlr.press/v97/qian19b.html>.

[24] R. GRAZZI, L. FRANCESCHI, M. PONTIL, AND S. SALZO, *On the iteration complexity of hypergradient computation*, in Proc. 37th ICML, vol. 119, 2020, pp. 3748–3758.

[25] R. GRAZZI, M. PONTIL, AND S. SALZO, *Nonsmooth implicit differentiation: deterministic and stochastic convergence rates*, in Proceedings of the 41st International Conference on Machine Learning, ICML’24, JMLR.org, 2024.

[26] J. HERTRICH, H. S. WONG, A. DENKER, S. DUCOTTERD, Z. FANG, M. HALTMEIER, ŽELJKO KERETA, E. KOBLER, O. LEONG, M. S. SALEHI, C.-B. SCHÖNLIEB, J. SCHWAB, Z. SHUMAYLOV, J. SULAM, G. S. WACHE, M. ZACH, Y. ZHANG, M. J. EHRHARDT, AND S. NEUMAYER, *Learning regularization functionals for inverse problems: A comparative study*, 2025, <https://arxiv.org/abs/2510.01755>.

[27] J. HOU, X. ZENG, S. CUI, X. JIANG, AND J. SUN, *Stochastic frank-wolfe algorithm for constrained bilevel optimization with improved per-iteration complexity*, IEEE Transactions on Signal Processing, 73 (2025), pp. 3237–3252, <https://doi.org/10.1109/TSP.2025.3596231>.

[28] A. KHALED AND P. RICHTÁRIK, *Better theory for SGD in the nonconvex world*, Trans. Mach. Learn. Res., (2023).

[29] P. KHANDURI, S. ZENG, M. HONG, H.-T. WAI, Z. WANG, AND Z. YANG, *A near-optimal algorithm for stochastic bilevel optimization via double-momentum*, in Proceedings of the 35th International Conference on Neural Information Processing Systems, NIPS ’21, Red Hook, NY, USA, 2021, Curran Associates Inc.

[30] D. P. KINGMA AND J. BA, *Adam: A method for stochastic optimization*, International Conference on Learning Representations (ICLR), (2015).

[31] H. LI AND Z. LIN, *Accelerated proximal gradient methods for nonconvex programming*, in Advances in Neural Information Processing Systems, C. Cortes, N. Lawrence, D. Lee, M. Sugiyama, and R. Garnett, eds., vol. 28, Curran Associates, Inc., 2015, https://proceedings.neurips.cc/paper_files/paper/2015/file/f7664060cc52bc6f3d620bc6dc94a4b6-Paper.pdf.

[32] D. MACLAURIN, D. DUVENAUD, AND R. P. ADAMS, *Gradient-based hyperparameter optimization through reversible learning*, 2015, <https://arxiv.org/abs/1502.03492>.

[33] S. MEHMOOD AND P. OCHS, *Automatic differentiation of some first-order methods in parametric optimization*, in Proceedings of the Twenty Third International Conference on Artificial Intelligence and Statistics, S. Chiappa and R. Calandra, eds., vol. 108 of Proceedings of Machine Learning Research, PMLR, 26–28 Aug 2020, pp. 1584–1594.

[34] S. MUKHERJEE, S. DITTMER, Z. SHUMAYLOV, S. LUNZ, O. ÖKTEM, AND C.-B. SCHÖNLIEB, *Data-driven convex regularizers for inverse problems*, in ICASSP 2024 - 2024 IEEE International Conference on Acoustics, Speech and Signal Processing (ICASSP), 2024, pp. 13386–13390, <https://doi.org/10.1109/ICASSP48485.2024.10447719>.

[35] P. OCHS, R. RANFTL, T. BROX, AND T. POCK, *Techniques for Gradient-Based Bilevel Optimization with Non-smooth Lower Level Problems*, Journal of Mathematical Imaging and Vision, 56 (2016), pp. 175–194, <https://doi.org/10.1007/s10851-016-0663-7>.

[36] P. OCHS, R. RANFTL, T. BROX, AND T. POCK, *Techniques for gradient based bilevel optimization with nonsmooth lower level problems*, 2016.

[37] F. PEDREGOSA, *Hyperparameter optimization with approximate gradient*, in Proceedings of The 33rd International Conference on Machine Learning, M. F. Balcan and K. Q. Weinberger, eds., vol. 48 of Proceedings of Machine Learning Research, New York, New York, USA, 20–22 Jun 2016, PMLR, pp. 737–746, <https://proceedings.mlr.press/v48/pedregosa16.html>.

[38] A. RAGHU, J. LORRAINE, S. KORNBLITH, M. McDERMOTT, AND D. DUVENAUD, *Meta-learning to improve pre-training*, in Proceedings of the 35th International Conference on Neural Information Processing Systems, NIPS ’21, Red Hook, NY, USA, 2021, Curran Associates Inc.

[39] Z. RAMZI, F. MANNEL, S. BAI, J.-L. STARCK, P. CIUCIU, AND T. MOREAU, *Shine: Sharing the inverse estimate from the forward pass for bi-level optimization and implicit models*, 2023, <https://arxiv.org/abs/2106.00553>.

[40] H. ROBBINS AND S. MONRO, *A stochastic approximation method*, The Annals of Mathematical Statistics,

22 (1951), pp. 400–407, <https://doi.org/10.1214/aoms/1177729586>.

[41] L. ROBERTS AND E. SMYTH, *A simplified convergence theory for byzantine resilient stochastic gradient descent*, EURO Journal on Computational Optimization, 10 (2022), p. 100038.

[42] S. M. ROBINSON, *Strongly regular generalized equations.*, Mathematics of Operations Research, 5 (1980), pp. 43–63.

[43] S. ROTH AND M. J. BLACK, *Fields of experts*, IJCV, 82 (2009), pp. 205–229.

[44] M. S. SALEHI, T. A. BUBBA, AND Y. KOROLEV, *Fast inexact bilevel optimization for analytical deep image priors*, in Scale Space and Variational Methods in Computer Vision, T. A. Bubba, R. Gaburro, S. Gazzola, K. Papafitsoros, M. Pereyra, and C.-B. Schönlieb, eds., Cham, 2025, Springer Nature Switzerland, pp. 30–42.

[45] M. S. SALEHI, S. MUKHERJEE, L. ROBERTS, AND M. J. EHRHARDT, *An adaptively inexact first-order method for bilevel optimization with application to hyperparameter learning*, SIAM Journal on Mathematics of Data Science, 7 (2025), pp. 906–936, <https://doi.org/10.1137/24M1653513>.

[46] M. S. SALEHI, S. MUKHERJEE, L. ROBERTS, AND M. J. EHRHARDT, *Bilevel learning with inexact stochastic gradients*, in Scale Space and Variational Methods in Computer Vision, T. A. Bubba, R. Gaburro, S. Gazzola, K. Papafitsoros, M. Pereyra, and C.-B. Schönlieb, eds., Cham, 2025, Springer Nature Switzerland, pp. 347–359.

[47] A. SHABAN, C.-A. CHENG, N. HATCH, AND B. BOOTS, *Truncated back-propagation for bilevel optimization*, in Proceedings of the Twenty-Second International Conference on Artificial Intelligence and Statistics, K. Chaudhuri and M. Sugiyama, eds., vol. 89 of Proceedings of Machine Learning Research, PMLR, 16–18 Apr 2019, pp. 1723–1732, <https://proceedings.mlr.press/v89/shaban19a.html>.

[48] F. SHERRY, M. BENNING, J. C. DE LOS REYES, M. J. GRAVES, G. MAIERHOFER, G. WILLIAMS, C.-B. SCHÖNLIEB, AND M. J. EHRHARDT, *Learning the sampling pattern for mri*, IEEE Transactions on Medical Imaging, 39 (2020), pp. 4310–4321.

[49] M. STAUDIGL, S. WEISSMANN, AND T. VAN LEEUWEN, *Derivative-free stochastic bilevel optimization for inverse problems*, 2024, <https://arxiv.org/abs/2411.18100>.

[50] E. SUONPERÄ AND T. VALKONEN, *Linearly convergent bilevel optimization with single-step inner methods*, Computational Optimization and Applications, 87 (2024), pp. 571–610, <https://doi.org/10.1007/s10589-023-00527-7>.

[51] E. SUONPERÄ AND T. VALKONEN, *Single-loop methods for bilevel parameter learning in inverse imaging*, Journal of Nonsmooth Analysis and Optimization, Volume 5 (2025), 5, <https://doi.org/10.46298/jnsao-2025-15577>.

[52] P. VICOL, L. METZ, AND J. SOHL-DICKSTEIN, *Unbiased gradient estimation in unrolled computation graphs with persistent evolution strategies*, in International Conference on Machine Learning, PMLR, 2021, pp. 10553–10563.